2008 IEEE International Conference on
Robotics and Automation
Pasadena, CA, USA, May 19-23, 2008

A Line-Based Obstacle Avoidance Technique for Dexterous Manipulator Operations

Nicholas A. Scott and Craig R. Carignan

Abstract— **Cameras are often used for visual servoing or real-time mapping of the external environment in both autonomous and teleoperated tasks with a dexterous manipulator. Nominal operations will likely produce manipulator configurations that occlude the line-of-sight from the camera to a target of interest. In this paper, a technique is developed that treats the camera line-of-sight as a virtual obstacle in order to prevent camera occlusion. The approach is based on using virtual point charges to represent obstacles and using the self-motion of the arm to avoid collisions. The approach is demonstrated on the Ranger Dexterous Manipulator.**

I. INTRODUCTION

During autonomous manipulator operations, real-time mapping of unknown and dynamic sampling environments require that the camera line-of-sight (LOS) to the target be maintained at all times. In Figure 1, the SAMURAI manipulator, shown mounted to the front end of the JAGUAR autonomous underwater vehicle, is being used to retrieve samples with the assistance of a pair of externally mounted cameras on the upper hull [12], [11]. An autonomous vision system called "AVATAR" uses stereo vision to identify and locate sample targets for retrieval and then sends position commands to the robot controller. The trajectory planner must ensure that the resulting manipulator configurations do not obstruct the camera LOS during the sampling operation.

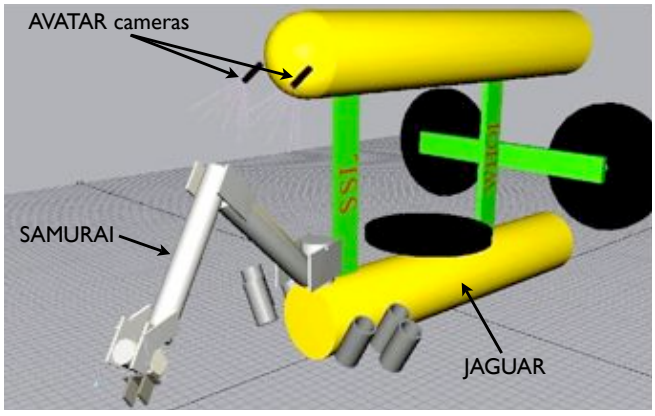

Fig. 1. Illustration showing SAMURAI manipulator mounted to lower hull of JAGUAR and AVATAR stereo cameras on upper hull.

N. Scott is formerly a graduate student with the Space Systems Laboratory at the University of Maryland and is now a research engineer with the National Institute of Standards and Technology, Gaithersburg, MD 20899 USA nicholas.scott@nist.gov

C. Carignan is an adjunct professor with the Dept. of Aerospace Engineering, University of Maryland, College Park, MD 20742 USA craigc@ssl.umd.edu

This paper discusses the design and implementation of a potential field-based obstacle avoidance system that uses manipulator self-motion to avoid collisions with obstacles. Camera occlusion is prevented by modeling the LOS from the camera to a point of interest as a virtual line obstacle. Though this paper focuses on preventing camera occlusion, this technique can be used in a variety of manipulation tasks that require real-time obstacle avoidance.

This paper begins with a brief survey of previous work in potential energy approaches to obstacle avoidance in Section II. Section III overviews the inverse kinematics and potential field models used in this work. Section IV provides a 3-link planar example and describes how line obstacles are modeled. Section V demonstrates this approach on an eight degree of freedom (DOF) manipulator. Conclusions are provided in Section VI.

II. PREVIOUS WORK

Manipulator obstacle avoidance is still an active area of research in robotics [10], [13], [8]. Current methods can be categorized into configuration-space (C-space) and energy-based approaches. Because of their computational complexity, C-space approaches are generally ill-suited for real-time obstacle avoidance in high-dimensional systems [2]. Energy-based approaches use artificial potential fields to guide the manipulator away from obstacles. Obstacles are modeled with high potential energy while obstacle-free regions are modeled with low potential energy. The manipulator configurations that lie in the valleys of the potential field are chosen to guide the manipulator away from obstacles. Energy-based approaches can be further divided into coupled and decoupled approaches.

The coupled approach, developed by Hogan, combines a potential field with an impedance controller [5]. Disturbance forces are generated from the potential field to guide the manipulator away from obstacles. This technique has shown promise in both low-dimensional [9] and high-dimensional systems developed at the Jet Propulsion Lab for space robotic applications [1]. This solution is advantageous because it provides a means of controlling the dynamic behavior of the manipulator as it interacts with obstacles by modifying the impedance controller gains. However, this solution couples the obstacle avoidance system with the control scheme which may not be desirable.

The decoupled approach, developed by Khatib, uses the negative gradient of the potential field to direct the self-motion of the manipulator towards a lower potential energy configuration for obstacle avoidance [6]. Unlike the coupled

approach, this solution is independent of the control scheme being used because it is implemented within the inverse kinematics. However, this approach does not produce a one-to-one mapping between the end-effector position and joint configuration because it is based on a local optimization of velocity.

Wang presents an extension to Khatib's approach that numerically searches for the local minimum potential energy solution instead of using a single step toward the minimum [17]. Since Wang's solution searches for a minimum in a potential field based solely on the position of the arm and obstacles, it results in unique joint solutions and yeilds "cyclic" motion [16]. Some promising results are presented for snake-like planar manipulators maneuvering through a cluttered point obstacle field. This paper extends Wang's approach to three-dimensions and also develops a method for incorporating line obstacles.

III. MANIPULATOR OBSTACLE AVOIDANCE

This section describes how locally minimum potential solutions are computed to simultaneously avoid obstacles, joint limits, and singularities. To this end, the total potential field, V, comprises three components:

$$\mathbf{V} = \mathbf{V_{obst}} + \mathbf{V_{jlim}} + \mathbf{V_{manip}} \tag{1}$$

V_{obst} is used to guide the manipulator away from obstacles, V_{jlim} is used to avoid joint limits, and V_{manip} is used to prevent singular configurations of the manipulator. Obstacles, joint limits, and singularities are modeled with high potential energy and are avoided by searching for a configuration q that minimizes the total potential energy subject to the end-effector constraints:

$$\min_{\mathbf{q}} \ \mathbf{V}, \ \mathbf{s.t.}\ \mathbf{x} = \mathbf{f(q)} \tag{2}$$

The function f defines the kinematic mapping from the joint configuration q to the end-effector position and orientation (pose) x.

For a desired change in the end-effector pose Δx, the minimum potential configuration is determined in three steps.

1) Calculate the pseudo-inverse solution

$$\mathbf{\Delta q_{pseudo}} = \mathbf{J^{\dagger}\Delta x} \tag{3}$$

where $J^{\dagger}$ is the right pseudo-inverse of the Jacobian and is defined as:

$$\mathbf{J^{\dagger}} \equiv \mathbf{J^T(JJ^T)^{-1}} \tag{4}$$

2) Calculate the nullspace component that minimizes the potential energy. Do this numerically by using a gradient-based search along the self-motion manifold. Beginning at the configuration from Step 1, compute each iteration using

$$\mathbf{\Delta q_i} = (\mathbf{I} - \mathbf{J_i^{\dagger}J_i})(-\nabla \mathbf{V(q_i)}) \tag{5}$$

where $-\nabla V(q_i)$ is the negative gradient of the potential field for the configuration at iteration i. I is an $N \times N$ identity matrix for a manipulator with N joints. The matrix $I - J_i^{\dagger}J_i$ projects the potential field gradient onto the self-motion manifold to ensure the end-effector location, satisfied in Step 1, does not change. The local minimum is found when Δq_i falls below a specified threshold $\Delta q_{threshold}$ and the resulting nullspace component is the sum of the joint displacements for each iteration:

$$\mathbf{\Delta q_{null}} = \sum_{\mathbf{i}} \mathbf{\Delta q_i} \tag{6}$$

3) Compute the final result by summing the pseudo-inverse solution and the nullspace component

$$\mathbf{\Delta q} = \mathbf{\Delta q_{pseudo}} + \mathbf{\Delta q_{null}} \tag{7}$$

A. Obstacle Potential: V_{obst}

An electric potential field is used to model the interaction between the obstacles and the manipulator. The obstacles are modeled as point charges and the major links of the manipulator (those with significant length) are modeled as charged line segments. The electric field E_{obst}, created by the point charge obstacles, repels the charged links of the manipulator as shown in Figure 2.

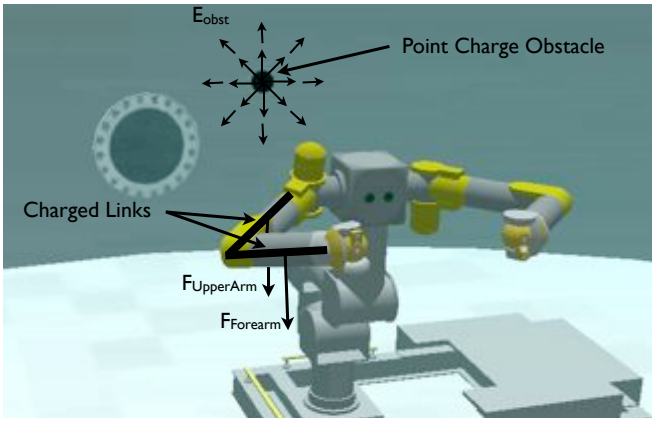

Fig. 2. A point charge obstacle creates an electric field E_{obst} which repels the line charge modeled links of the manipulator.

The obstacle potential energy at position R is

$$\mathbf{V_{obst}(R)} = -\int_{\infty}^{\mathbf{R}} \mathbf{E_{obst}(R)dL} \tag{8}$$

where L is an arbitrary path. The negative gradient yields:

$$-\nabla \mathbf{V_{obst}(R)} = \mathbf{E_{obst}(R)} \tag{9}$$

For a point charge obstacle at R' with charge Q', the electric field at R is

$$\mathbf{E_{obst}(R)} = \frac{\mathbf{Q'}}{\mathbf{4\pi\epsilon_o}} \frac{\mathbf{R - R'}}{\mathbf{|R - R'|^3}} \tag{10}$$

where ϵ_o is the dielectric permittivity of free-space.

The interaction between a point charge obstacle and line segment charge link of the manipulator can be projected onto a plane as shown in Figure 3. A point charge Q' is located at position O which produces an electric field E. The

electric field produces a force and moment on the charged line segment with endpoints P_1 and P_2. The origin of the coordinate frame is affixed to P_2 as shown. The x-axis points in the direction of P_1 to P_2 and the y-axis points in the direction of P_{min} to O, where P_{min} is the closest point on the line containing P_1 and P_2 to O. The values for scalars a, b, and c are defined in Table I. The sign of a and b depend on the relative position of the charged line segment and point charge, while the sign of c is always positive.

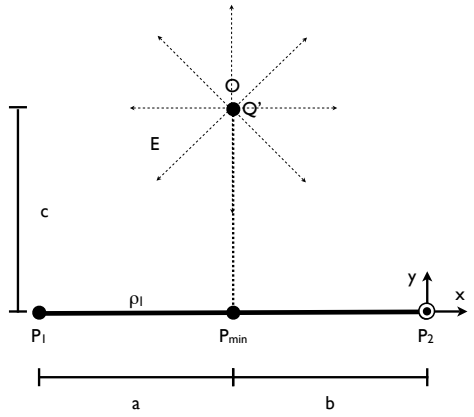

Fig. 3. Force and moment on a charged line segment due to a point charge.

TABLE I
FORCE-MOMENT CALCULATION VARIABLE DESCRIPTIONS.

Value	Description	Range
a	Distance P_{min} to P_1 in -x-direction	$-\infty < a < +\infty$
b	Distance P_{min} to P_2 in +x-direction	$-\infty < b < +\infty$
c	Distance P_{min} to O in +y-direction	$0 < c < +\infty$

The force on the line segment due to the electric field is calculated by integrating the electric field from (10) over the charged line segment with charge density ρ_l:

$$\mathbf{F} = \frac{\mathbf{Q'}\rho_\mathbf{l}}{\mathbf{4\pi\epsilon_o}} \int_\mathbf{l} \frac{\mathbf{R} - \mathbf{R'}}{|\mathbf{R} - \mathbf{R'}|^\mathbf{3}} \mathbf{dl} \tag{11}$$

Using $R = x\hat{x}$ and $R' = -b\hat{x} + c\hat{y}$ and performing the integration yields

$$\mathbf{F_x} = \mathbf{k_{obst}}\left(\frac{\mathbf{1}}{\sqrt{\mathbf{a^2 + c^2}}} - \frac{\mathbf{1}}{\sqrt{\mathbf{b^2 + c^2}}}\right) \tag{12}$$

$$\mathbf{F_y} = \mathbf{k_{obst}}\left(-\frac{\mathbf{a}}{\mathbf{c}\sqrt{\mathbf{a^2 + c^2}}} - \frac{\mathbf{b}}{\mathbf{c}\sqrt{\mathbf{b^2 + c^2}}}\right) \tag{13}$$

where $k_{obst} = \frac{Q'\rho l}{4\pi\epsilon_o}$ for an actual electric field in free-space. However, for the artificial potential field, selection of k_{obst} provides a means of varying the influence of the point charge obstacle on the manipulator.

Multiplying the force by the moment arm and integrating over the length of the segment yields the moment about the origin on the charged line segment:

$$\mathbf{M} = \mathbf{k_{obst}}\left(\frac{\mathbf{ab - c^2}}{\mathbf{c}\sqrt{\mathbf{a^2 + c^2}}} - \frac{\mathbf{-b^2 - c^2}}{\mathbf{c}\sqrt{\mathbf{b^2 + c^2}}}\right)\hat{\mathbf{z}} \tag{14}$$

The planar force and moment from (12), (13), and (14) are represented in 3D by using the homogeneous transform between the planar coordinate frame in Figure 3 and a frame in the manipulator task space [4]. Multiplying the 3D link force and moment by the transpose of the Jacobian yields the resulting joint torques:

$$\tau_\mathbf{j} = \mathbf{J_j^T}\mathcal{F}_\mathbf{j} \tag{15}$$

$\mathcal{F}_j$ is a partitioned vector containing the force and moment vectors for link j. J_j is the partitioned Jacobian matrix containing both the translational and rotational Jacobians for the first j links. τ_j is the vector of joint torques for all joints prior to link j. For a fixed-base manipulator, the force and moment on link j is only reacted in the joints prior to link j. Thus, the transpose of the Jacobian J_j can be used to transform the Cartesian forces and moments $\mathcal{F}_j$ on link j into joint torques τ_j for all joints from the base to link j.

For a general scenario with many point obstacles, (15) is applied to each obstacle and link combination and the results are summed to produce a net joint torque vector that describes the influence of all obstacles on the manipulator. Thus the negative gradient of the obstacle potential field mapped into joint space is

$$\tau_\mathbf{obst} = -\nabla\mathbf{V_{obst}}(\mathbf{q}) = \sum_{\mathbf{i=1}}^{\mathbf{M}} \sum_{\mathbf{j=1}}^{\mathbf{N}} \mathbf{J_j^T}\mathcal{F}_\mathbf{ij} \tag{16}$$

where M is the number of obstacles, N is the number of major links of the manipulator, and $\mathcal{F}_{ij}$ is the force on link j due to obstacle i. The dimensions of τ_{obst} vary with j so care must be taken when summing the vectors, but this is a straightforward formulation.

B. Joint Limit Potential: V_{jlim}

Without an opposing force, the obstacle potential field will cause the joints of the manipulator to migrate towards their limits subject to the end-effector constraints. To prevent this, a joint limit potential field is added which models each joint as a spring to push the joints towards their centers of travel:

$$\mathbf{V_{jlim}}(\mathbf{q}) = \frac{\mathbf{1}}{\mathbf{2}}(\mathbf{q} - \mathbf{q_o})^\mathbf{T}\mathbf{K}(\mathbf{q} - \mathbf{q_o}) \tag{17}$$

K is a diagonal matrix of spring constants and q_o is the nominal equilibrium position for the joints. The negative gradient yields the joint torques on the manipulator due to the field:

$$\tau_\mathbf{jlim} = -\nabla\mathbf{V_{jlim}}(\mathbf{q}) = \mathbf{K}(\mathbf{q_o} - \mathbf{q}) \tag{18}$$

To account for differences in joint ranges, each diagonal entry in K is defined as:

$$\mathbf{K_{ii}} = \frac{\mathbf{k_{jlim}}}{\mathbf{\Delta q_i}} \tag{19}$$

where Δq_i is the range for joint i and k_{jlim} is a single parameter that can be used to adjust the influence of the joint limit potential field on the manipulator.

C. Manipulability Potential: V_{manip}

To implement this algorithm on a real manipulator, singularity avoidance is needed. Singularities occur when the matrix being inverted in (4) becomes singular, or equivalently when the manipulability $D \equiv |JJ^T|$ becomes zero [4]. Singularities can be avoided by using:

$$\mathbf{V_{manip}(q)} = -\mathbf{k_{manip}}(|\mathbf{JJ^T}|)^{\frac{1}{2}} \tag{20}$$

Though the potential energy is always negative, the shape of the potential field is what matters. When singular, the potential is at a maximum at zero. When the manipulator is far from a singularity, the potential is negative. Thus, driving the manipulator towards a lower potential configuration produces the desired singularity avoidance behavior.

The negative gradient of (20) gives the resulting joint torques on the manipulator due to the singularity potential field:

$$\tau_{\mathbf{manip}} = -\nabla \mathbf{V_{manip}(q)} = \frac{\mathbf{k_{manip}}}{\mathbf{2}(|\mathbf{JJ^T}|)^{\frac{1}{2}}} \nabla \mathbf{D} \tag{21}$$

The total influence of all the potential fields is produced by summing the joint torques from each field

$$\tau = -\nabla \mathbf{V(q)} = \tau_{\mathbf{obst}} + \tau_{\mathbf{jlim}} + \tau_{\mathbf{manip}} \tag{22}$$

where the components are given by (16), (18), and (21). The total joint torque is used in (5) to search for the minimum potential solution.

IV. PLANAR 3-LINK MANIPULATOR EXAMPLE

This section demonstrates a 3-link planar manipulator subject to a single point charge and discusses the line charge obstacle model. Though the obstacle avoidance technique described in Section III applies to a general 3D case, a planar manipulator is used in this section to more clearly demonstrate the approach.

A. Planar 3-Link Manipulator with One Point Obstacle

Consider the planar 3-link example shown in Figure 4. The left picture shows the manipulator in a non-singular starting configuration at q^T = [0 1.57 -1.57] radians with one point obstacle placed near link 3 at position $(1.5, 1.3)$ meters. The influence coefficients k_{obst}, k_{jlim}, and k_{manip} are all set to 0.1. All three joints have a nominal position at zero and a joint range of $[-\pi, \pi]$ radians. The lengths for all three links are set to 1 meter and $\Delta q_{threshold}$ is set to 0.001 radians.

Table II shows the joint torques produced by each potential field. Since the obstacle is close to link 3 of the manipulator, the joint torques due to the obstacle potential field are dominant and are consistent with moving each link downward away from the obstacle. The torques due to the joint limits are small and consistent with returning the manipulator to its nominal zero configuration. The singularity potential produces negligible torques since the manipulator is not near a singularity.

The picture on the right in Figure 4 shows the local minimum potential configuration at q^T = [-0.36 1.79 -1.07] radians after iterating over (5). The manipulator is driven away from the point obstacle while maintaining the end-effector position.

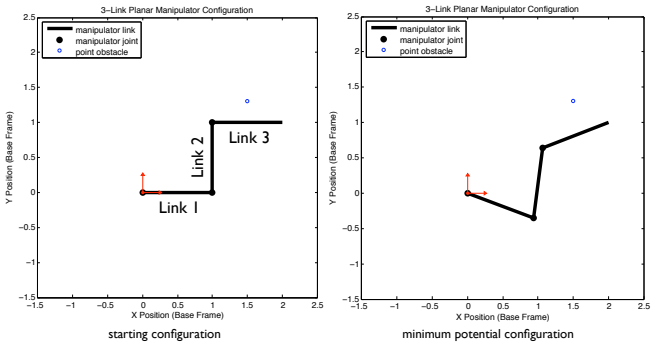

Fig. 4. Obstacle avoidance for a planar 3-link manipulator.

TABLE II

JOINT TORQUES DUE TO POTENTIAL FIELDS.

Joint Torques			
Source	τ_1 (Nm)	τ_2 (Nm)	τ_3 (Nm)
obstacles	0	0	0
joint limits	0	-0.0250	0.0250
singularities	$\sim$0	$\sim$0	$\sim$0
total	$\sim$0	-0.0250	0.0250

B. Line Obstacle Model

A line obstacle is desirable for modeling a camera's LOS to a target of interest. Incorporating line segment obstacles into the potential field calculations was initially investigated, but proved to be exceedingly complex. Alternatively, a simpler approach was chosen to approximate the line obstacle with a series of point obstacles which allows the same calculations from Section III to be used. The points chosen on the line segment obstacle are the points closest to each link of the manipulator as shown in Figure 5 for a 3-link planar manipulator. OB_1, OB_2, and OB_3 are the points closest to links 1, 2, and 3 respectively. The points of closest approach are updated in real-time and their locations change as the manipulator and line obstacles move.

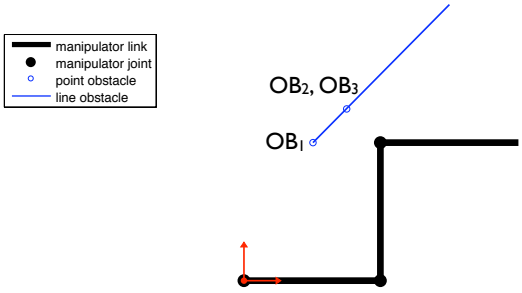

Fig. 5. Line obstacle approximation using the points of closest approach.

Though observations from this research have shown promising results using this line obstacle model, a single point charge obstacle may not be sufficient for all scenarios. Alternatively, more points along the line obstacle could be chosen to provide a more accurate model. The points of

closest approach were chosen for this research in an attempt to minimize the computational complexity and simplify the implementation.

V. MANIPULATOR IMPLEMENTATION AND DEMONSTRATION

The 8-DOF Ranger Dexterous Manipulator uses a partitioned inverse kinematics scheme which segments the manipulator at the wrist [3]. The first 4-DOFs are used to position the arm and the last 4-DOFs are used to orient the end-effector. The self-motion of the arm is represented by the "orbit" of the elbow about the shoulder-wrist vector SW (shown in Figure 6) while the position of the wrist and shoulder are held fixed [15], [7]. The orbital angle ϕ is defined as the angle that the plane formed by the points S, E, and W makes with a reference plane.

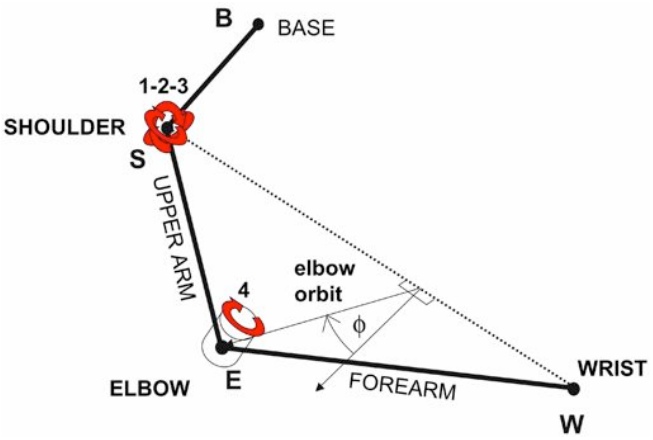

Fig. 6. Definition of shoulder-elbow-wrist (SEW) angle.

The elbow orbit can often be used to avoid collisions of the arm links with obstacles as the end-effector follows a prescribed path. A flowchart that demonstrates how the collision avoidance is incorporated into the inverse kinematics is shown in Figure 7. The end-effector (tool) pose is commanded through a set of hand controllers or a trajectory system and is used to calculate the pseudo-inverse solution. Obstacle positions stored in a world model are combined with joint telemetry to produce the nullspace component. The pseudoinverse solution is then combined with the nullspace component to produce the local minimum potential arm configuration.

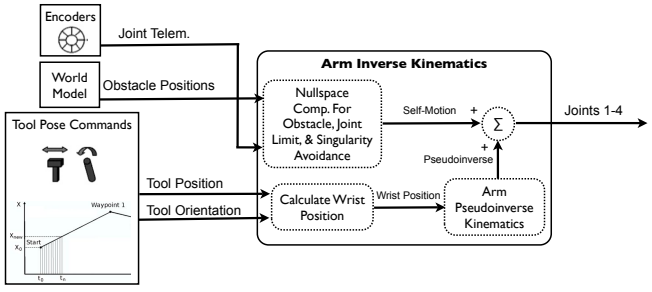

Fig. 7. Inverse kinematics flowchart for Ranger Mk. II manipulator.

To demonstrate successful occlusion avoidance, a mock sampling scenario was setup as shown in Figure 8. A video camera was affixed to the head of the manipulator support stand and pointed towards a yellow rubber duck sample target. The points of closest approach, OB_1 and OB_2, used to approximate the LOS obstacle are shown for the pictured configuration. For this demonstration, the location of the camera LOS was measured by hand and entered into the world model. In real operations, the vision system would determine the position of the sample target which would define the LOS.

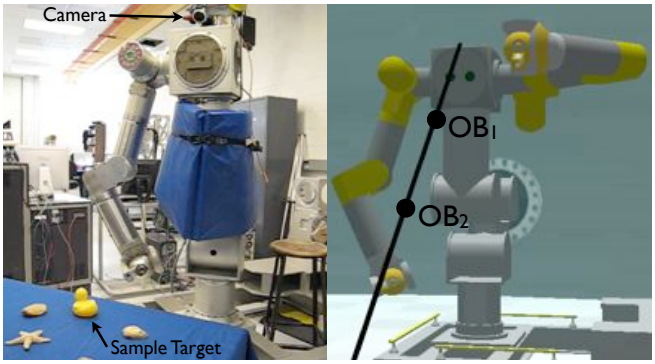

Fig. 8. Experimental setup for Ranger which shows an external view (left) and a simulated view with the modeled camera LOS and the corresponding points of closest approach (right).

The end-effector was commanded to move above the camera LOS and then downward in a fashion which would normally cause the forearm to occlude the camera. A sequence of snapshots in Figure 9 shows the manipulator movement as well as the view from the camera. As the end-effector moves above the LOS from Position 1 to Position 2 there is little self-motion since the links do not occlude the view. However, when the end-effector moves downward to Position 3 the forearm nears the LOS obstacle and the SEW angle is modified to prevent occluding the camera view to the sample target.

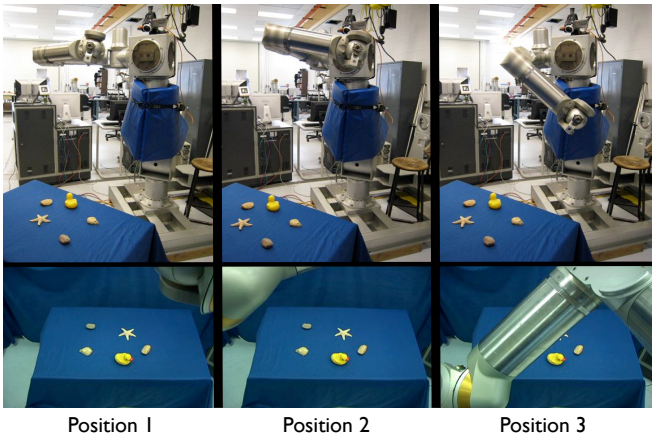

Fig. 9. External view (top row) and camera view (bottom row) during LOS avoidance maneuver.

Figure 10 shows a plot of the obstacle distance to each

link. OB_1 and OB_2 are the points on the line obstacle closest to the manipulator's upper arm link and forearm link respectively. OB_1 and OB_2 are continually updated in real-time during the trajectory to reflect the current manipulator configuration and line obstacle position. The point of closest approach approximation is sufficient for the obstacle avoidance system to successfully maintain a distance of at least 5 centimeters from each link during the trajectory and avoid occlusion.

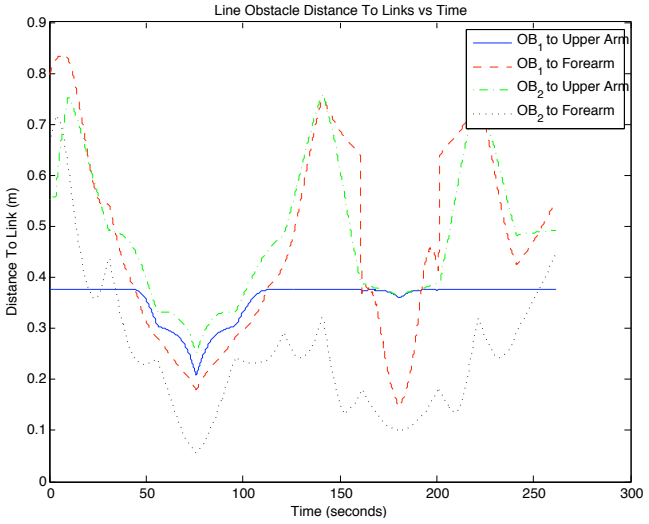

Fig. 10. Obstacle distance to Ranger links during LOS avoidance maneuver. OB_1 is closest to the upper arm. OB_2 is closest to the forearm.

VI. CONCLUSION

This paper discussed the development of a real-time obstacle avoidance scheme to prevent camera occlusion for visually guided manipulators in dynamic environments. The decoupled energy-based scheme provides a flexible real-time system that can easily be adapted to existing manipulators. This scheme was based on Wang's methodology which uses an electric potential field to model obstacles and iterates to find a local minimum potential solution. This work extended Wang's work to three-dimensions, provided a model for incorporating line obstacles, added singularity avoidance, and was successfully demonstrated on an 8-DOF manipulator.

Though successful, some limitations of this approach were observed. High joint velocities were commanded in some situations due to the interaction between the obstacle and joint limit potential fields. These circumstances caused a sudden change in the shape of the potential field and resulted in a large shift in the minimum potential solution. A joint velocity limiting scheme was used to slow these transients, though another method to better control the dynamic behavior is desired. Also, the point of closest approach approximation for line obstacles needs to be further refined. When a line obstacle becomes parallel with a link, the point of closest approach becomes undefined. For this paper, the midpoint of the line obstacle was chosen, however in some situations this caused instability because of a discontinuous jump in the obstacle position [14].

Efforts are underway to develop an approach for using this same obstacle avoidance system for kinematically non-redundant manipulators by attaching a virtual prismatic link between the end-effector and the desired trajectory. Using the same methodology developed in this paper, the virtual link adds redundancy and allows the end-effector to deviate from the commanded path in order to avoid obstacles. This method can also be used to allow end-effector deviations from the nominal path for kinematically redundant manipulators.

ACKNOWLEDGMENTS

The authors would like to thank Stephen Roderick and Joseph Lisee for their invaluable software support for this work. This project was sponsored by the NASA Astrobiology Science and Technology for Exploring the Planets (ASTEP) program under grant #NNG04GB31G.

REFERENCES

[1] B. Bon and H. Seraji, "On-line collision avoidance for the ranger telerobotic flight experiment," in *Proceedings of the 1996 IEEE International Conference on Robotics and Automation*, 1996.

[2] J. F. Canny, "The complexity of robot motion planning," in *MIT Press*, 1988.

[3] C. R. Carignan and R. D. Howard, "A partitioned redundancy management scheme for an eight-joint revolute manipulator," *Journal of Robotic Systems*, vol. 17, no. 9, pp. 453–468, 2000.

[4] J. J. Craig, *Introduction to Robotics Mechanics and Control*, 3rd ed. Pearson Prentice Hall, 2005.

[5] N. Hogan, "Impedance control: An approach to manipulation. part iii: Application," *ASME Journal of Dynamic Systems Measurement and Control*, vol. 107, pp. 17–24, 1985.

[6] O. Khatib, "Real-time obstacle avoidance for manipulators and mobile robots," *The International Journal of Robotics Research*, vol. 5, no. 1, pp. 90–98, 1986.

[7] K. Kreutz-Delgado, M. Long, and H. Seraji, "Kinematic analysis of 7 dof manipulators," *Int. Journal of Robotics Research*, vol. 11, no. 5, pp. 469–481, 1992.

[8] J. Y. Lee and H. Choset, "Sensor-based planning for planar multi-convex rigid bodies," in *In Proceedings of the 2005 International Conference on Robotics and Automation*, 2005.

[9] S. Lee, S.-Y. Yi, J.-O. Park, and C.-W. Lee, "Reference adaptive impedance control and its application to obstacle avoidance trajectory planning," in *Proceedings of 1997 IROS*, 1997.

[10] C.-C. Lin, L.-W. Kuo, and J.-H. Chuang, "Potential-based path planning for robot manipulators," *Journal of Robotic Systems*, 2005.

[11] M. P. Naylor, "Autonomous target recognition and localization for manipulator sampling tasks," Master's thesis, University of Maryland, College Park, 2006.

[12] M. P. Naylor, N. A. Scott, E. Atkins, and S. Roderick, "Towards autonomous sampling and servicing with the ranger dexterous manipulator," in *Proceedings of the AIAA Infotech@Aerospace Conference*, September 2005.

[13] R. V. Patel, F. Shadpey, F. Ranjbaran, and J. Angeles, "A collision-avoidance scheme for redundant manipulators: Theory and experiments," *Journal of Robotic Systems*, 2005.

[14] N. A. Scott, "A line-based obstacle avoidance technique for dexterous manipulator operations," Master's thesis, University of Maryland, College Park, 2007.

[15] H. Seraji, "Configuration control of redundant manipulators: Theory and implementation," *IEEE Transactions on Robotics and Automation*, vol. 5, no. 4, Aug. 1989.

[16] C.-C. Wang and V. Kumar, "On singular behaviors of impedance-based repeatable control for redundant robots," *Journal of Robotic Systems*, vol. 18, no. 4, pp. 171–186, 2001.

[17] C.-C. Wang, V. Kumar, and G.-M. Chiu, "A motion control and obstacle avoidance algorithm for hyper-redundant manipulators," in *Proceedings of 1998 International Symposium on Underwater Technology*. IEEE, April 1998.